Journal of Applied Physics ARTICLE pubs.aip.org/aip/jap

A fully automatized method for the unambiguous wavelength-by-wavelength determination of the thickness and optical property of a very thin film with a transparent range

Cite as: J. Appl. Phys. **134**, 045301 (2023); doi: 10.1063/5.0150135
Submitted: 12 March 2023 · Accepted: 5 July 2023 ·
Published Online: 24 July 2023

Florian Maudet,[1,a)] Charlotte Van Dijck,[1] Muhammad Hamid Raza,[1] and Catherine Dubourdieu[1,2]

AFFILIATIONS

[1]Helmholtz-Zentrum-Berlin für Materialien und Energy GmbH, Institute "Functional Oxides for Energy Efficient Information Technology," Hahn-Meitner Platz 1, 14109 Berlin, Germany
[2]Freie Universität Berlin, Physical Chemistry, Arnimallee 22, 14195 Berlin, Germany

[a)]**Author to whom correspondence should be addressed:** maudet.florian@yahoo.fr

ABSTRACT

Spectroscopic ellipsometry is a powerful method with high surface sensitivity that can be used to monitor the growth of even sub-monolayer films. However, analysis of ultrathin films is complicated by the correlation between the dielectric constant and thickness. This problem is usually resolved by fixing one or the other value, limiting the information that can be extracted. Here, we propose a method to determine unambiguously the refractive index, extinction coefficient, and thickness of a film when a transparent range is available in the energy range investigated. We decompose the analysis in three steps. First, the thickness of the film is determined from the transparent range of the film. Then, knowing the thickness of the layer, an initial estimation of the refractive index and extinction coefficient is made based on a first-order Taylor expansion of the ellipsometric ratio. Finally, using this estimation, a numerical iteration is done to ensure convergence of the fit toward the solution. A theoretical example of the method is given for two different thicknesses of TiO_2 films. Finally, the method is applied to the experimental data measured during the atomic layer deposition of a thin film of $Hf_{0.5}Zr_{0.5}O_2$ grown on Si. The thickness, refractive index, and extinction coefficient are retrieved with high precision (respectively, 0.01 and 0.002) in the energy range of 3.5–6.5 eV. A detailed analysis is presented on the accuracy of the retrieved values and their dependency on random and systematic errors for different energy ranges.

I. INTRODUCTION

Spectroscopic ellipsometry is an optical, non-destructive, characterization method commonly used to precisely monitor the growth of thin films, both in research and industry.[1] This method relies on the measurement of a complex ellipsometric ratio, ρ, that characterizes the changes in polarization after polarized light interacts with a sample. As opposed to spectrophotometry and other techniques, an ellipsometry measurement is made without the need to calibrate the background intensity, an aspect that consequently enhances the reliability of the measurement.[2] Furthermore, owing to its high sensitivity to surface change and low footprint, the method is particularly suited for *in situ* study.[3] In the simple case of an isotropic three-phase configuration consisting of the ambient (with complex refractive index $\tilde{n}_a$), thin film ($\tilde{n}_f$) and substrate ($\tilde{n}_s$), ellipsometry allows to determine the unknown thickness d_f and dielectric constant of the thin film $\tilde{\varepsilon}_f = (\tilde{n}_f)^2 = (n_f + ik_f)^2$ where $\tilde{n}_f$, n_f, and k_f are the complex refractive index, real refractive index, and extinction coefficient of the thin film, respectively. Commonly, the retrieval of d_f and $\tilde{n}_f$ from the measured ρ is made by developing an optical model assuming a certain dispersion property of the dielectric constant.[1] Indeed, due to the non-linearity of the optical equations, no direct inversion can be made.[4] The information is retrieved by varying the parameters of the optical model to minimize the mean square error (MSE) that

characterizes the error between the measured and modeled data. Therefore, a prior estimation of the optical properties is needed to ensure the convergence of the model toward a realistic solution. This method can lead to incorrect optical properties when spectral features of the film, that were not anticipated and therefore absent from the model, are overlooked. This is the case, for example, for a sample with sub-bandgap absorption features that would not have been taken into account with a simple Tauc–Lorentz model.[5] Furthermore, in the case of a very thin film ($\frac{d_f}{\lambda} \ll 1$ with λ being the wavelength), this approach cannot be applied as $\tilde{n}_f$ and d_f become strongly correlated.[2] This is particularly problematic for the very first steps of the growth of a thin film. This issue is usually overcome by fixing either d_f or $\tilde{n}_f$. For example, to study an atomic layer deposited (ALD) film, it is common to fix the optical property of a growing film to the bulk value and to recover information on film growth from the thickness evolution.[6–9] However, in addition to preventing us from retrieving information on the dielectric constant of the film, this method leads to incorrect values of thickness, in the case of ultrathin films (typically below 10 nm), as $\tilde{n}_f$ depends on the film thickness (an ultrathin film of, e.g., 0.8 nm has a refractive index different from the one of the bulk).

One way to avoid this issue is to use complementary measurements to disambiguate d_f and $\tilde{n}_f$, such as measuring the mass of the deposited material with a quartz crystal microbalance.[10] Another method was developed relying on the simultaneous measurement of changes in the reflected intensity and ρ to disambiguate d_f and $\tilde{n}_f$.[11] A drawback is the need for a precise measurement of the intensity as it dominates the measurement accuracy.[11] Another approach solely relying on the measurement of ρ was developed by minimizing the presence of artifacts from the substrate in the dielectric constant for incorrect thicknesses.[12,13] This method allows to unambiguously determine the thickness when a substrate presents a sharp feature, i.e., with a high variation with energy, like a critical point. An a priori knowledge of $\tilde{n}_f$ is, however, necessary to ensure the convergence toward the correct solution as multiple solutions of $\tilde{n}_f$ coexist for a given d_f.[4] Finally, when the material is transparent ($k_f = 0$), $\tilde{n}_f$ is a real, at least on part of the investigated spectral range, a direct inversion of the thickness and refractive index can be made.[14] The method was extended recently to take into account the error on d_f, enhancing the accuracy.[15] Knowing d_f, $\tilde{n}_f$ can then be calculated for the whole spectral range by mapping all existing solutions and selecting the physically reasonable solution.[16] This step is computationally intensive and requires a manual selection of the solution to ensure that a physical solution is found. It limits the applicability of real-time analysis of a growing film. Therefore, a point-by-point method to unambiguously determine d_f and $\tilde{n}_f$ without prior assumption on $\tilde{n}_f$ or manual selection of the solution is desirable to study the growth of very thin films *in situ* and in real-time.

In this paper, we develop a deterministic algorithm that can be used to unambiguously determine d_f, n_f, and k_f of very thin films (< 10 nm)—where a transparent range is available—solely relying on standard ellipsometric data. To the best of our knowledge, such a mathematical method has not been reported so far. We decompose the analysis in two steps. First, the ambiguity between the thickness of the film and the optical constant is removed following the procedure developed by Gilliot *et al.*[15] Then, knowing the thickness of the layer, the refractive index and extinction coefficient are determined through a first-order Taylor expansion of the ellipsometric ratio ρ, ensuring wavelength by wavelength convergence of n_f and k_f to the correct solution from a numerical iterative refinement.[17] A theoretical example is presented for a thin film of TiO_2. Detailed analysis and discussion on the error of d_f, n_f, and k_f for different thicknesses of TiO_2 are presented. Finally, the method is demonstrated for the practical example of a very thin film of $Hf_{0.5}Zr_{0.5}O_2$ (HZO) grown by ALD.

II. MODEL AND METHOD TO UNAMBIGUOUSLY DETERMINE $\tilde{n}_f$ AND d_f

The method can be divided into three parts: a first part to determine the thickness of the film, a second one to have an estimation of the optical properties from the calculated thickness, and a third one that uses this estimation to ensure convergence toward the actual solution by a numerical iteration. Here, we consider the simple case of an isotropic three-layer configuration: ambient ($\tilde{n}_a$), thin film ($\tilde{n}_f$), and substrate ($\tilde{n}_s$) as illustrated in Fig. 1.

The experimentally measured ellipsometric ratio is given by[1]

$$\rho_e = \frac{r_p}{r_s} = \tan \psi_e e^{-i\Delta_e}, \tag{1}$$

where ψ_e and Δ_e are the measured ellipsometric angles, r_p and r_s are the p and s polarized complex reflection coefficients of the stack, respectively. These coefficients are given by

$$r_p = \frac{r_{af,p} + r_{fsub,p}X}{1 + r_{af,p}r_{fsub,p}X} \quad \text{and} \quad r_s = \frac{r_{af,s} + r_{fsub,s}X}{1 + r_{af,s}r_{fsub,s}X}, \tag{2}$$

with

$$X = e^{\frac{j4\pi d_f \sqrt{\tilde{n}_f^2 - \tilde{n}_a^2 \sin^2 \theta_i}}{\lambda}}, \tag{3}$$

where $r_{af,p(s)}$, $r_{fsub,p(s)}$ are the Fresnel reflection coefficients of the ambient/thin film interface and the thin film/substrate interface of p (s) polarization, respectively. It should be noted that we are using the physics convention $\tilde{n}_f = n_f + ik_f$ leading to the negative sign in Eq. (1) and its absence in Eq. (3).[1] In the case of a very thin film, $\tilde{n}_f$ and d_f are highly correlated, and cannot be disambiguated with these equations only.[10]

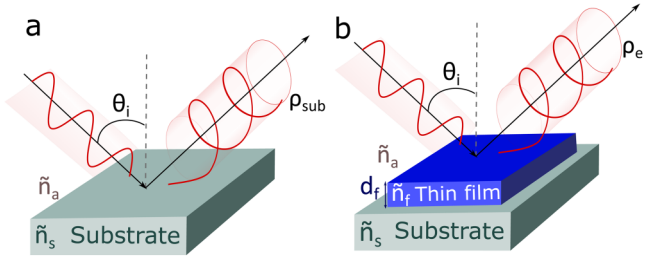

FIG. 1. Schematic of an ellipsometry measurement on a bare substrate (a) and in three-phase ambient/thin film/substrate configuration (b).

A. Thickness and refractive index disambiguation for very thin films

In order to disambiguate $\tilde{n}_f$ and d_f, we rely on the method that was presented by Gilliot *et al.* and that we remind here below.[15] In this method, we first consider the transparent range of the thin film. Therefore, $\tilde{n}_f$ is a real number, i.e., $\tilde{n}_f = n_f$. From Eq. (3), $\tilde{d}_f$ can be expressed as

$$\tilde{d}_f = \frac{-j\lambda \ln(X) + 2m\lambda\pi}{4\pi\sqrt{n_f^2 - \tilde{n}_a^2 \sin^2\theta_i}}, \tag{4}$$

where θ_i is the angle of incidence and m is an integer that takes into account the multiplicity of orders due to the periodic behavior of X. In the case of very thin films, $m = 0$.

From there, the goal is to calculate an expression of X, that is independent of $\tilde{d}_f$, in order to express $\tilde{d}_f(n_f)$ from Eq. (4). Using Eqs. (1) and (2), it follows that

$$\begin{aligned}\rho_e &= \frac{\dfrac{r_{af,p} + r_{fsub,p}X}{1 + r_{af,p}r_{fsub,p}X}}{\dfrac{r_{af,s} + r_{fsub,s}X}{1 + r_{af,s}r_{fsub,s}X}} \\ &= \frac{r_{af,p} + r_{af,p}r_{af,s}r_{fsub,s}X + r_{fsub,p}X + r_{fsub,p}r_{af,s}r_{fsub,s}X^2}{r_{af,s} + r_{fsub,s}X + r_{af,p}r_{fsub,p}r_{af,s}X + r_{af,p}r_{fsub,p}r_{fsub,s}X^2},\end{aligned} \tag{5}$$

$$\begin{aligned}&(\rho_e r_{af,p}r_{fsub,p}r_{fsub,s} - r_{fsub,p}r_{af,s}r_{fsub,s})X^2 \\ &+ (\rho_e r_{fsub,s} + \rho r_{af,p}r_{fsub,p}r_{af,s} - r_{af,p} - r_{fsub,p})X \\ &+ \rho_e r_{af,s} - r_{af,p} = 0.\end{aligned} \tag{6}$$

From Eq. (6), for a given n_f two solutions of X can be found independently of $\tilde{d}_f$. Consequently, using those solutions, two values of $\tilde{d}_f(n_f)$ can be calculated.

Now that we can express the thickness in a function of the refractive index, the main idea of the procedure is that as both the refractive index and thickness must be real numbers, the correct value of n_f is the one that cancels out the imaginary part of the thickness, such that

$$Im\left(\tilde{d}_f(n_f)\right) = 0. \tag{7}$$

These two values of $\tilde{d}_f(n_f)$ can be numerically computed for the whole wavelength (or energy) range with the method described in.[16] To do so, the values of $\tilde{d}_f$ are computed for a broad range of n_f values, typically $n_f = [1 - 10]$ with 100 steps. Approximated values of n_f are given by those values corresponding to the change in the sign of the imaginary part of $\tilde{d}_f$. From these initial approximations, the precise values of n_f are then finally computed using an algorithm to find the root of Eq. (7). The algorithm used in this study is the Newton–Raphson method.[18] The sign ambiguity in the solution of Eq. (6) is solved by keeping the solution that makes physical sense ($d_f > 0$).

The error of d_f can be calculated from the propagation error formula as follows:[19]

$$\begin{aligned}\sigma_{d_f} = \Bigg\{ &\left(\frac{\partial d_f}{\partial \psi}\right)^2 \sigma_\psi^2 + \left(\frac{\partial d_f}{\partial \Delta}\right)^2 \sigma_\Delta^2 + \left(\frac{\partial d_f}{\partial \theta_i}\right)^2 \sigma_{\theta_i}^2 + \left(\frac{\partial d_f}{\partial n_{sub}}\right)^2 \sigma_{n_{sub}}^2 + \left(\frac{\partial d_f}{\partial k_{sub}}\right)^2 \sigma_{k_{sub}}^2 + \left(\frac{\partial d_f}{\partial \lambda}\right)^2 \sigma_\lambda^2 \\ &+ 2\left(\frac{\partial d_f}{\partial \psi}\right)\left(\frac{\partial d_f}{\partial n_{sub}}\right)\sigma_{\psi n_{sub}}^2 + 2\left(\frac{\partial d_f}{\partial \Delta}\right)\left(\frac{\partial d_f}{\partial n_{sub}}\right)\sigma_{\Delta n_{sub}}^2 \\ &+ 2\left(\frac{\partial d_f}{\partial \psi}\right)\left(\frac{\partial d_f}{\partial k_{sub}}\right)\sigma_{\psi k_{sub}}^2 + 2\left(\frac{\partial d_f}{\partial \Delta}\right)\left(\frac{\partial d_f}{\partial k_{sub}}\right)\sigma_{\Delta k_{sub}}^2 \\ &+ 2\left(\frac{\partial d_f}{\partial \psi}\right)\left(\frac{\partial d_f}{\partial \theta_i}\right)\sigma_{\psi\theta_i}^2 + 2\left(\frac{\partial d_f}{\partial \Delta}\right)\left(\frac{\partial d_f}{\partial \theta_i}\right)\sigma_{\Delta\theta_i}^2 \\ &+ 2\left(\frac{\partial d_f}{\partial \psi}\right)\left(\frac{\partial d_f}{\partial \lambda}\right)\sigma_{\psi\lambda} + 2\left(\frac{\partial d_f}{\partial \Delta}\right)\left(\frac{\partial d_f}{\partial \Delta}\right)\sigma_{\Delta\lambda}, \Bigg\}\end{aligned} \tag{8}$$

where σ_j is the standard deviation of the associated parameter j and σ_{xy}^2 is the covariance of the parameters x, y.

As this computation is made for all the measured wavelengths, d_f and σ_{d_f} can be presented as a function of energy (E). Although the measurements are usually made with a fixed wavelength step, the results will be discussed as a function of energy since this scale is more relevant to discuss the material properties like bandgap.

The computation presented above allows us to determine d_f unambiguously from any energy points of the measured data. As it is a thickness, d_f should be constant for all energies. However, two causes can explain the energy dependency of d_f:

- This computation is made with the hypothesis that $k_f = 0$; therefore, d_f will vary in the energy range where this is not true.
- Measurements inevitably contain errors that cause variation of d_f with the energy. Evaluating the impact of the errors of the measurement on d_f is thus critical to evaluate the range of energy, where it can be accurately determined.[15]

Consequently, d_f has to be determined from the region where $d_f(E)$ is constant.

Once the thickness is known in theory, it is possible to directly calculate $\tilde{n}_f$. However, knowing d_f is not sufficient to determine n_f and k_f from ellipsometric measurements since multiple solutions of $\tilde{n}_f$ coexist for a given thickness.[4]

B. A deterministic algorithm to extract the thickness, refractive index, and extinction coefficient automatically

From the point-by-point thickness inversion of Eq. (7), a measurement will give multiple values of thickness for the different energies. Rather than a manual selection of the thickness, we propose here to extract the thickness automatically. The multiple solutions observed in $d_f(E)$ are caused by the measurement error and non-transparency of the thin film. Therefore, by looking at the energy range where σ_{d_f} and $\left|\frac{\partial d}{\partial E}\right|$ are minimum, the thickness can be accurately evaluated. We calculate the thickness as a weighted average of $d_f(E)$ with the weights $w(E)$. The weights are calculated to minimize the values of σ_{d_f} and $\left|\frac{\partial d}{\partial E}\right|$ using the following function:

$$w(E) = \frac{1}{\left|\frac{\partial d_f(E)}{\partial E}\right| \sigma_{d_f}(E)}. \tag{9}$$

At this step, we have determined $d_f(E)$ unambiguously from $\tilde{n}_f$ with an algorithm that can be applied automatically.

In theory, by knowing d_f, $\tilde{n}_f$ can be unambiguously determined by computing all the possible solutions that reproduce the measured data using Eqs. (1)–(3). However, without further process, manual work is still needed to select the correct couple of values of n_f and k_f among the multiple solutions. We propose here an algorithm to automatize this process. In order to remove the need for the manual selection of solutions n_f and k_f, we first compute an initial guess of their value. This method was proposed recently by Jung *et al.*[17] to approximate $\tilde{n}_f$ without any *a priori* knowledge in the case of very thin films $\left(\frac{d_f}{\lambda} \ll 1\right)$. It relies on the first-order Taylor expansion of ρ. They evidenced that, in such a configuration, $\tilde{n}_f$ can be approximated by

$$\tilde{n}_f^2 \approx \frac{1}{2}\left(\tilde{n}_a^2 + \tilde{n}_{sub}^2 + \frac{\delta_\rho}{\alpha}\right) \pm \frac{1}{2}\sqrt{\left(\tilde{n}_a^2 + \tilde{n}_{sub}^2 + \frac{\delta_\rho}{\alpha}\right)^2 - 4\tilde{n}_a^2\tilde{n}_{sub}^2}, \tag{10}$$

with

$$\alpha = 4i\frac{2\pi}{\lambda} d_f \frac{\tilde{n}_a\tilde{n}_{sub}^2\cos(\theta_i)\sin^2(\theta_i)}{\left(\tilde{n}_a - \tilde{n}_{sub}^2\right)\left(\tilde{n}_{sub}^2 - \tilde{n}_a^2 + \left(\tilde{n}_a^2 + \tilde{n}_{sub}^2\right)\cos(2\theta_i)\right)} \tag{11}$$

and

$$\delta_\rho = \frac{\rho_e - \rho_{sub}}{\rho_{sub}}, \tag{12}$$

where ρ_{sub} is the ellipsometric ratio of the substrate before thin film deposition [Fig. 1(a)]. It can be either measured before thin film deposition or simulated from the known $\tilde{n}_{sub}$. The ambiguity in the sign can be removed by choosing the solution that is the closest to the refractive index as determined from Eq. (7) in the transparent range of the film. Since the aforementioned method to determine $\tilde{n}_f$ is a first-order approximation, there will necessarily be a residual error between the modeled ellipsometric ratio ρ_m [that can be calculated from Eq. (5)] and ρ_e. To minimize it, a point-by-point numerical iteration can be made to refine the determination of $\tilde{n}_f$. To this end, an iterative method to reduce the error, such as the Newton–Raphson method, can be used as described in the supplementary material. After this numerical iteration, we have unambiguously determined $n_f(E)$, $k_f(E)$, and d_f. Further work could be done to ensure the physicality of the values by implementing an algorithm to enforce Kramers–Kronig consistent values of $n_f(E)$, $k_f(E)$, and also to ensure $k_f(E) > 0$. However, to avoid making the method presented here too complicated, we will refer the reader to a previous work, where the implementation of these aspects is presented.[16]

Finally, an important aspect of this method is to estimate the error $\sigma_{\tilde{n}_f}$ on n_f and k_f to be able to discriminate physical features of the spectra from a measurement artifact. We apply again the propagation error formula leading to the following error expression:[19]

$$\sigma_{\tilde{n}_f} = \sqrt{\begin{aligned}
&\left(\frac{\partial\tilde{n}_f}{\partial\psi}\right)^2\sigma_\psi^2 + \left(\frac{\partial\tilde{n}_f}{\partial\Delta}\right)^2\sigma_\Delta^2 + \left(\frac{\partial\tilde{n}_f}{\partial d_f}\right)^2\sigma_{d_f}^2 + \left(\frac{\partial\tilde{n}_f}{\partial n_{sub}}\right)^2\sigma_{n_{sub}}^2 + \left(\frac{\partial\tilde{n}_f}{\partial k_{sub}}\right)^2\sigma_{k_{sub}}^2 + \left(\frac{\partial\tilde{n}_f}{\partial\lambda}\right)^2\sigma_\lambda^2 \\
&+2\left(\frac{\partial\tilde{n}_f}{\partial\psi}\right)\left(\frac{\partial\tilde{n}_f}{\partial\theta_i}\right)\sigma_{\psi\theta_i} + 2\left(\frac{\partial\tilde{n}_f}{\partial\Delta}\right)\left(\frac{\partial\tilde{n}_f}{\partial\theta_i}\right)\sigma_{\Delta\theta_i} + 2\left(\frac{\partial\tilde{n}_f}{\partial\psi}\right)\left(\frac{\partial\tilde{n}_f}{\partial d_f}\right)\sigma_{\psi d_f} \\
&+2\left(\frac{\partial\tilde{n}_f}{\partial\Delta}\right)\left(\frac{\partial\tilde{n}_f}{\partial d_f}\right)\sigma_{\Delta d_f} + 2\left(\frac{\partial\tilde{n}_f}{\partial d_f}\right)\left(\frac{\partial\tilde{n}_f}{\partial\theta_i}\right)\sigma_{d_f\theta_i} + 2\left(\frac{\partial\tilde{n}_f}{\partial\psi}\right)\left(\frac{\partial\tilde{n}_f}{\partial n_{sub}}\right)\sigma_{\psi n_{sub}} + 2\left(\frac{\partial\tilde{n}_f}{\partial\Delta}\right)\left(\frac{\partial\tilde{n}_f}{\partial n_{sub}}\right)\sigma_{\Delta n_{sub}} \\
&+2\left(\frac{\partial\tilde{n}_f}{\partial\psi}\right)\left(\frac{\partial\tilde{n}_f}{\partial k_{sub}}\right)\sigma_{\psi k_{sub}} + 2\left(\frac{\partial\tilde{n}_f}{\partial\Delta}\right)\left(\frac{\partial\tilde{n}_f}{\partial k_{sub}}\right)\sigma_{\Delta k_{sub}} + 2\left(\frac{\partial\tilde{n}_f}{\partial d_f}\right)\left(\frac{\partial\tilde{n}_f}{\partial n_{sub}}\right)\sigma_{d_f n_{sub}} + 2\left(\frac{\partial\tilde{n}_f}{\partial d_f}\right)\left(\frac{\partial\tilde{n}_f}{\partial k_{sub}}\right)\sigma_{d_f k_{sub}} \\
&+2\left(\frac{\partial\tilde{n}_f}{\partial\psi}\right)\left(\frac{\partial\tilde{n}_f}{\partial\lambda}\right)\sigma_{\psi\lambda} + 2\left(\frac{\partial\tilde{n}_f}{\partial\Delta}\right)\left(\frac{\partial\tilde{n}_f}{\partial\Delta}\right)\sigma_{\Delta\lambda} + 2\left(\frac{\partial\tilde{n}_f}{\partial d_f}\right)\left(\frac{\partial\tilde{n}_f}{\partial\lambda}\right)\sigma_{d_f\lambda}.
\end{aligned}} \tag{13}$$

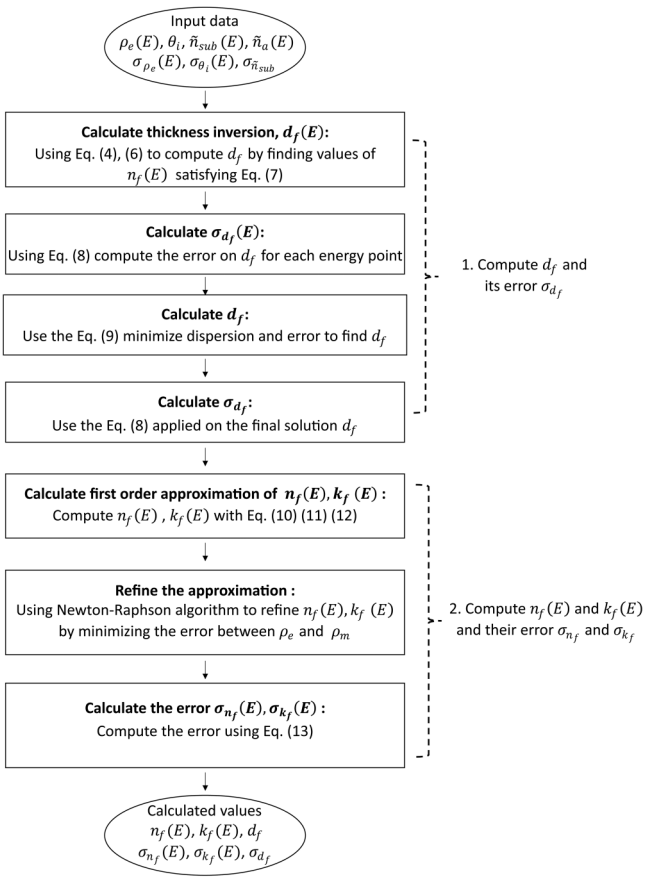

FIG. 2. Flow chart describing the steps and their goals for the proposed method.

It must be noted that, here, all errors are considered as random noise produced by the measurement. This is not the case, for example, for an error on θ_i that should be regarded as a systematic error, a fixed deviation inherent to the measurement configuration and which does not depend on energy. However, considering only random errors allows us to evaluate their impact on different parts of the energy spectrum. By having a look at the error, this point-by-point method allows to explicitly evaluate the accuracy of ellipsometry on the determination of d_f, n_f, and k_f for the whole spectral range. This information is useful in itself as it can be used, for instance, to evaluate if a spectral feature like a small absorption below the bandgap has a physical origin or if it sits in a range of low accuracy and could then be associated with the error of the measurement. The possibility to analyze the error on the whole spectral range is an asset of this method, as a similar evaluation is a hard task to do when the analysis is made with a modeled dispersion law like with Tauc–Lorentz oscillators.

The maximum thin film thickness that will lead to correct values of $\tilde{n}_f$ with this method depends on the error of thefirst-order approximation. If this error is too large, the numerical iteration will converge toward an incorrect solution.

To help understand the proposed method, we sum up the algorithmic steps in the following flow chart (Fig. 2):

The algorithm is available in the form of a Python code at https://doi.org/10.5281/zenodo.7722620 alongside example notebooks.

III. THEORETICAL EXAMPLE: A VERY THIN FILM OF TiO_2 ON Si

To illustrate the method, we first evaluate it with the theoretical case of a very thin film of $d_f = 1.00$ nm, of amorphous TiO_2 on a silicon substrate, for the energy range of 0.77–6.20 eV simulated for an incident angle of $\theta_i = 65°$. TiO_2 is chosen as an example because it has a transparent range in the energy range considered here. Its dispersion law is modeled by a Tauc–Lorentz model (A = 256.08 eV, Br = 1.77 eV, E_0 = 4.00 eV, E_g = 3.40 eV, $\varepsilon_\infty = 1$) and the optical properties of the silicon substrate are taken from Ref. 20. To evaluate the uncertainty of the measurement, here, we consider relatively low, but realistic errors of $\sigma_\psi = \sigma_\Delta = \sigma_{\theta_i} = 0.01°$ $\sigma_\lambda = 0.1$ nm and errors of $\sigma_{n_{sub}} = \sigma_{k_{sub}} = 0.001$.

In Fig. 3(a), the thickness resulting from the McCrakin inversion of this stack is presented together with the calculated thickness from Eq. (9) with their respective error.

As expected, the thickness from the McCrakin inversion shows an energy dependence for values that are above the bandgap of TiO_2 ($k_f \neq 0$). Indeed, for this part of the spectrum, the hypothesis of a transparent film is not valid, and this range can, therefore, not be used to determine the thickness. This inversion has, therefore, already provided interesting information on the dielectric constant of the film that can be used to confirm the values of $\tilde{n}_f$. A region with $k_f \neq 0$ should reflect in a dispersive d_f. Below the bandgap, the inversion leads to an exact match with the actual value of the thickness. The error distribution with energy also provides valuable information. It shows that the error on d_f exponentially increases with decreasing energy in the low energy range (2.0–0.8 eV). This is due to the fact that for decreasing energy, the difference between ρ_{sub} and ρ_e also decreases, therefore, leading to a higher sensitivity to the measurement parameter errors σ_ψ, σ_Δ, σ_{θ_i}, σ_λ, and $\sigma_{\tilde{n}_{sub}}$, and to errors in ρ_e. The best energy range to accurately determine d_f is, therefore, in this case, 2.0–3.4 eV. Using Eq. (9) and the error evaluation in Eq. (8), a precise determination of $d_f = 1.00 \pm 0.03$ nm is achieved.

From the thickness value, a first estimation of n_f and k_f is then made from Eq. (10) and presented in Figs. 3(b) and 3(c) (red curves). The initial estimation is a relatively good approximation of the dispersion law of TiO_2. However, we observe a higher difference between the actual values and estimated ones for a higher energy than for a lower energy range where both values converge. The estimation is based on the first-order Taylor expansion, relying on the hypothesis that $\left(\frac{d_f}{\lambda} \ll 1\right)$; hence, the error will be increasingly small for decreasing energy (increasing wavelength) as the first-order expansion becomes a more accurate approximation. Using this first estimation, the error is then minimized by reducing the error between the measured and modeled ρ values with a Newton–Raphson algorithm. The values of n_f and k_f after the numerical iteration are presented in Figs. 3(b) and 3(c) (blue

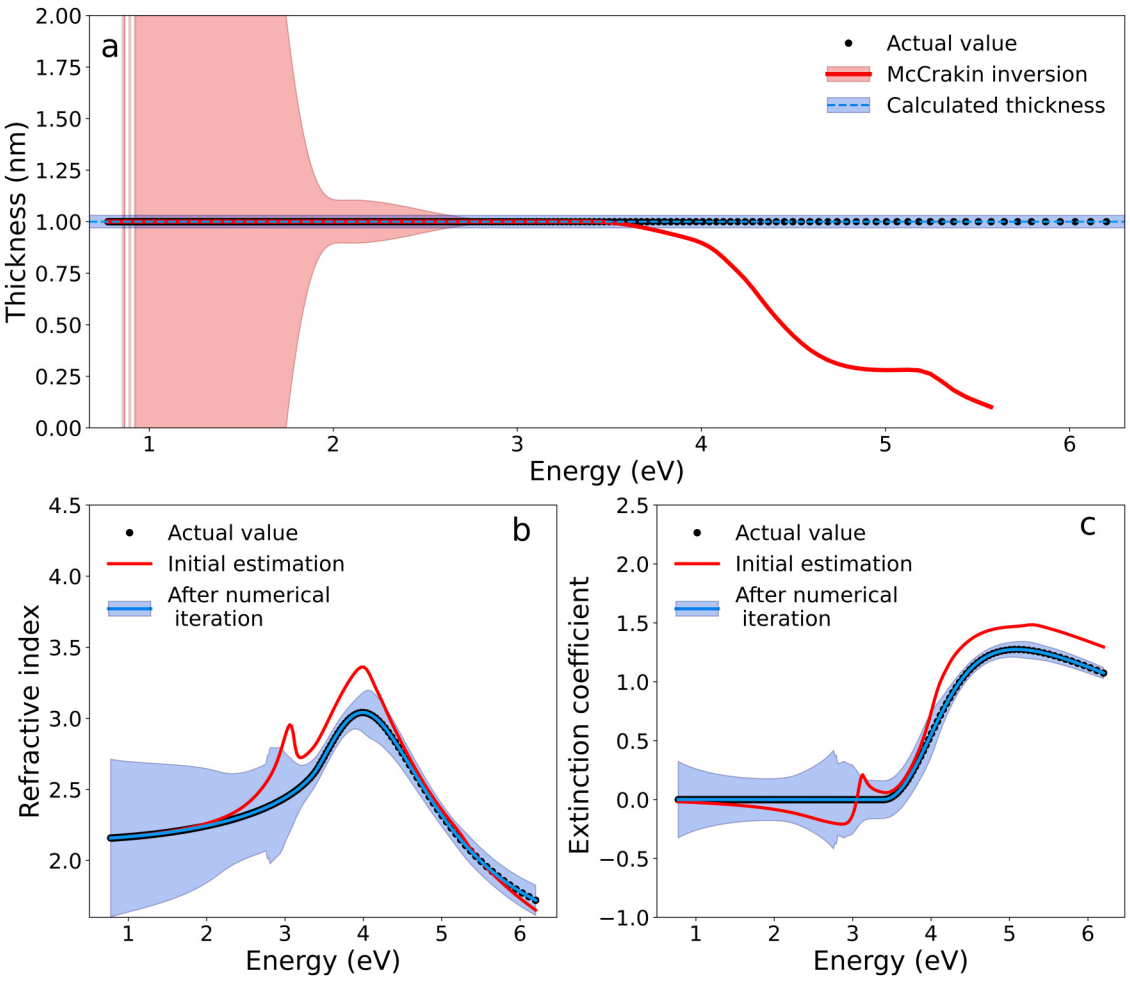

FIG. 3. (a) Thickness dependence on energy for a thin film of 1 nm (black dots) TiO_2 on silicon as determined by a McCrakin inversion method (red line) and calculated from Eq. (9) (blue dashed line). Dispersion law of the refractive index (b) and extinction coefficient (c) of TiO_2 (black dots) initial estimation from Eq. (10) (red line) and after the numerical iteration (blue line). The colored areas are the calculated errors on the respective values.

curves) with their respective errors represented by the colored areas. After the numerical iteration, the dispersion law of TiO_2 can be perfectly recovered. Regarding the errors on n_f and k_f, a relatively low error is observed in both cases in the high energy range (> 3.5 eV), while a large one is observed for the low energy range (< 3.5 eV). Indeed, for decreasing energy, δ_ρ decreases, leading to a higher sensitivity to the errors. Around 3 eV, the observed jump in the error is due to the proximity of the two solutions expressed in Eq. (10). Indeed, a small variation of the initial value of the numerical iteration will lead to the divergence of the fit toward one solution or the other. Consequently, the error on n_f and k_f is large in the low energy range.

We then considered a thin TiO_2 film of $d_f = 5.00$ nm, keeping everything else the same. The results are presented in Fig. 4.

Due to the increased thickness, the error on the McCrakin inversion is reduced and an accurate determination can, therefore, be made in a larger energy range from 1.5 to 3.4 eV [Fig. 4(a)]. The calculated thickness from Eq. (9) is $d_f = 5.00 \pm 0.02$ nm. The error on the thickness is much smaller than in the previous case ($d_f = 1.00$ nm) due to a lower dependence on the measurement error as 5 nm leads to a larger difference on δ_ρ. The initial estimation of n_f and k_f is, however, quite different from the actual value [Figs. 4(b) and 4(c)]. This is expected as the first-order Taylor expansion that leads to a larger error for thicker films. The numerical iteration, however, leads to a very accurate determination of n_f and k_f with a very low error on the considered energy range also due to a higher δ_ρ.

With these two examples, we show that d_f, n_f, and k_f can be unambiguously determined with the determination of the thickness

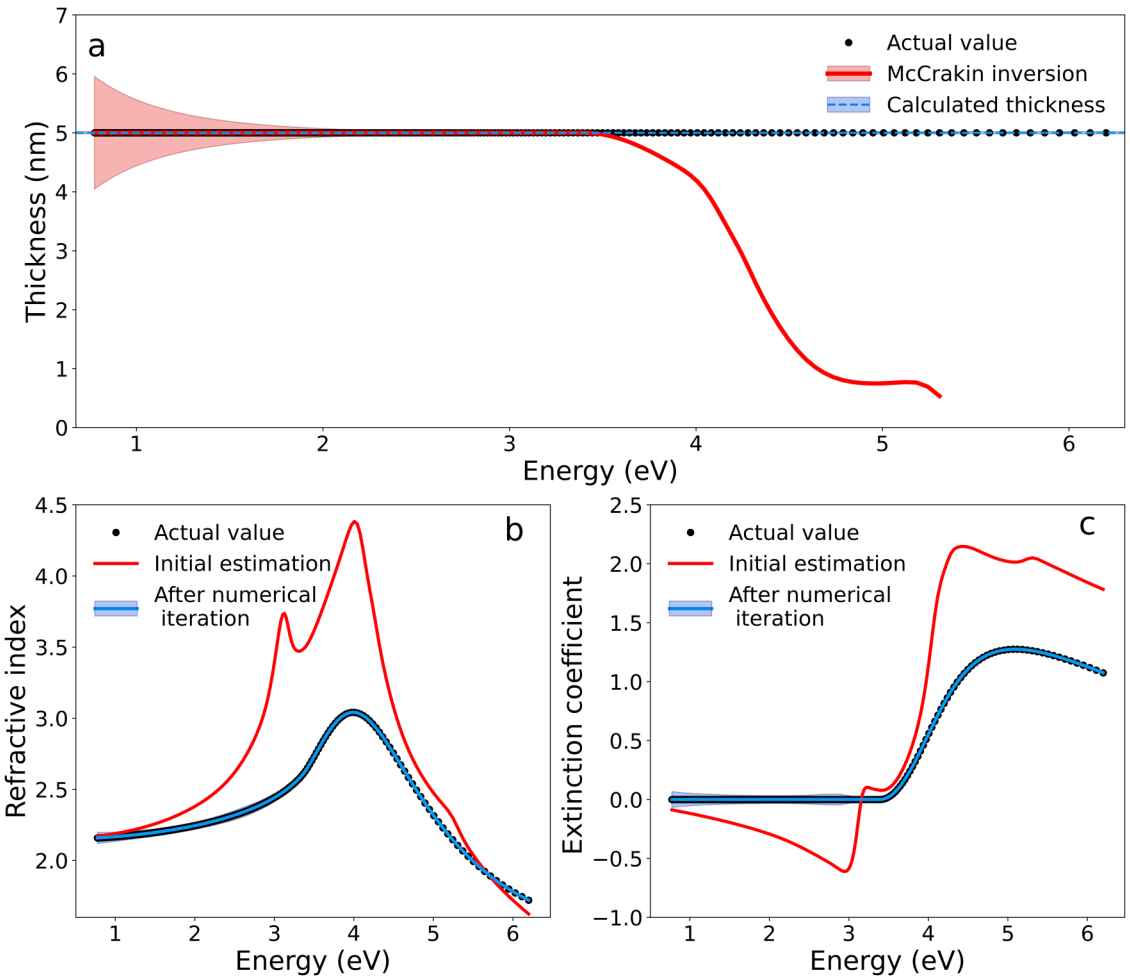

FIG. 4. (a) Thickness dependence on energy for a thin film of 5.00 nm (black dots) TiO_2 on silicon as determined by a McCrakin inversion method (red line) and calculated from Eq. (9) (blue dashed line). Dispersion law of the refractive index (b) and extinction coefficient (c) of TiO_2 (black dots) initial estimation from Eq. (10) (red line) and after numerical iteration (blue line). The colored areas are the calculated errors on the respective values.

being made without any assumption on the n_f value. However, in the case of ultrathin films (1 nm), the n_f and k_f values cannot be determined below a given energy (here 3.4 eV), as the error becomes too large.

In the second part of the supplementary material, we present the result of our method for a broader range of thickness of TiO_2 (0.2–10 nm). We demonstrate that it can be applied to successfully retrieve d_f, n_f, and k_f automatically, where a manual standard modeling approach fails even when considering data with multiple angles of incidence.

It should also be noted that as illustrated in the supplementary material, above a certain film thickness, the method will lead to incorrect values of $\tilde{n}_f$ due to a high error of the first-order approximation. The initial values n_f and k_f, would then, indeed, lead the numerical iteration to converge toward one of the incorrect solutions. In this example of a thin film of TiO_2 on Si, a thickness larger than 10 nm leads to an incorrect convergence of n_f and k_f.

IV. EXPERIMENTAL EXAMPLE: A THIN FILM OF HZO ON Si

As an experimental example, we applied the method to the study of a thin $Hf_{0.5}Zr_{0.5}O_2$ film grown by atomic layer deposition on RCA-cleaned silicon (cf. Sec. VI). As a native oxide of SiO_x is present on the surface of Si, the SiO_x/Si substrate was measured before the deposition to determine ρ_{sub}. Then, to calculate $\tilde{n}_{sub}$, the pseudo-dielectric constant function was calculated.[1] This method allows us to replace a sample that consists of multiple layers with a pseudo-dielectric constant that represents the dielectric property of this stack and can thus be considered as the dielectric constant of a

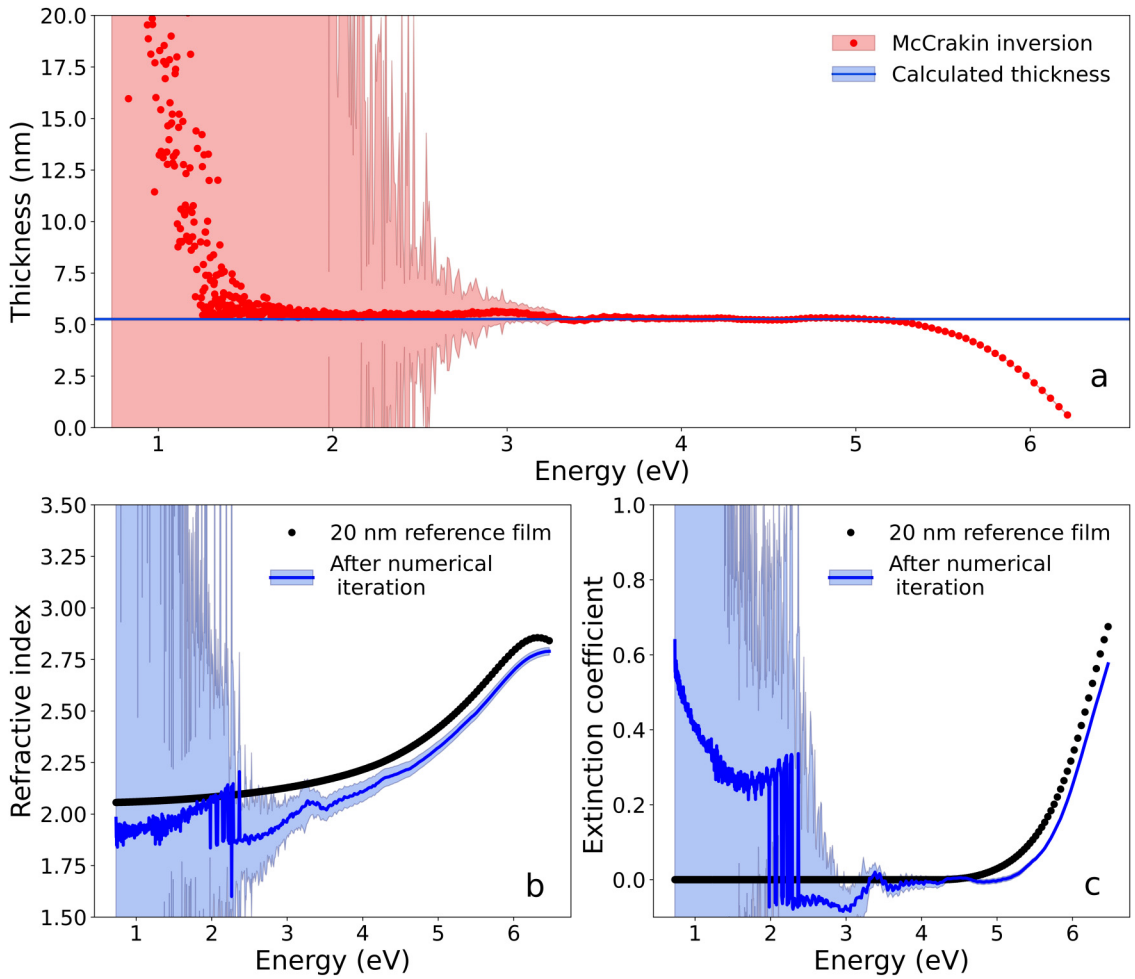

FIG. 5. (a) Thickness dependence on energy for a ∼5 nm HZO film deposited on an RCA cleaned silicon substrate as determined by a McCrakin inversion method (red line) and calculated from Eq. (9) (blue line) – Dispersion curves of (b) the refractive index and (c) extinction coefficient determined from the proposed method (blue lines) together with the curves for a 20 nm HZO film (black dots). The colored areas are the calculated error on the respective values.

new semi-infinite substrate.[21] The errors $\sigma_\psi$and σ_Δ were determined from five measurements of ψ and Δ on the sample. The error $\sigma_{\theta_i} = 0.1^\circ$ on the angle offset was estimated from five measurements of a 25 nm SiO_2 reference sample on Si. The error $\sigma_{\tilde{n}_{sub}}$ on $\tilde{n}_{sub}$was calculated from the measurements of five RCA-cleaned substrates. The resulting calculated thickness d_f is presented in Fig. 5(a).

Three regions are observed for the thickness from the McCrakin inversion [Fig. 5(a)]. First, there is an energy-dependent region at high energy (∼5.2–6.5 eV). This region corresponds to the non-transparent range of the thin film and cannot be used for the determination of the thickness. Then, a region of constant thickness with low error (∼2.5–5.2 eV) is observed from which the thickness can be accurately determined. A third region is observed at low energy (∼0.7–2.5 eV). In this region, the thickness values show a much larger error and also evolve with both the contribution of a higher scattering and an exponential increase of decreasing energy. As the thickness values are not solely randomly scattered, we can conclude that the observed exponential increase of the thickness comes from systematic errors, such as a constant offset in θ_i, or an error on the dispersion law of $\tilde{n}_{sub}$. A detailed analysis of this region could be done to exploit this artifact to correct for the systematic errors, for example, considering adding an offset of 0.1° to the angle of incidence to minimize the thickness evolution with energy. This is, however, outside the scope of this paper. Using Eqs. (9) and (8), we calculate the thickness of the film and its corresponding error to be $d_f = 5.27 \pm 0.06$ nm. We can, therefore, reach a very low uncertainty on the measured thickness, thanks to the presence of an energy range with high accuracy in the McCrakin inversion (∼2.5–5.2 eV).

In Figs. 5(b) and 5(c), the resulting n_f and k_f values are presented together with the values of a 20 nm thick HZO film. For high energies (> 3.0 eV), we show that both n_f and k_f have

dispersion curves similar to their thicker counterpart and that high accuracy ($\sigma_{\tilde{n}_{sub}} \leq 0.01 + 0.002i$) is achieved in both cases. The dispersion law is similar to a dispersion modeled by a Tauc–Lorentz function. Such a dispersion law is characteristic of amorphous materials for which the bandgap is present in the measured spectral region.[1] Note that we obtain such a dispersion law here with this point-by-point method without relying on a model of the dispersion law. The refractive index of the very thin film is lower (2.11 at an energy of 4.0 eV) than the one of the 20 nm film reference (2.21 at an energy of 4.0 eV), which is attributed to a lower density.[1] Using Bruggeman effective medium approximation, assuming the film is composed of HZO and nanometric air inclusions, we calculate that the very thin HZO film exhibits a density of around 85% of that of the 20 nm reference.[22] This is understood by the ALD growth mechanism that tends to generate gaps for the first step of growth due to steric hindrance.[23] Moreover, from the extinction coefficient, a shift toward higher energy of the exponential rise is observed for the thinner film compared to the 20 nm reference film. This shift leads to a higher bandgap (5.2 eV) compared to the reference sample (4.9 eV). The increased bandgap of the very thin film can be explained by a quantum confinement effect. Indeed, if the dimension of a material is of the same magnitude as the de Broglie wavelength of the electron wave function, it will generate a quantum confinement effect. This effect has already been observed during the growth of very thin films.[24]

For energies below ~3 eV, the error becomes large, which does not allow to conclude on the optical properties of the HZO thin film. At these energies, similar to the determination of the thickness, the dispersion laws present errors that are mostly produced from systematic errors of the measurement.

Therefore, at the present state, the proposed method can be applied to accurately measure d_f and $\tilde{n}_f$ of very thin films for an energy range higher than ~3 eV. It should be noted that the measurement of a thicker film will widen the energy range, where $\tilde{n}_f$ can be retrieved with high accuracy, as evidenced previously (Sec. III).

V. CONCLUSION

In this paper, we demonstrated a fully automated mathematical method to unambiguously determine the thickness, refractive index, and extinction coefficient of a very thin film with high accuracy, for energies typically larger than ~3 eV. The method is developed for thin films which present a range of transparency and are deposited on a substrate with known optical properties in the investigated energy range. The method is decomposed into three steps. First, the thickness is estimated from a McCrakin inversion by carefully looking at the energy range with minimal error and thickness dispersion. Second, a first estimation of the refractive index and extinction coefficient is done based on a first-order Talyor expansion of ρ. Finally, from this initial estimation and the calculated thickness, convergence toward the correct solution of $\tilde{n}_f$ is ensured with a wavelength-by-wavelength numerical iteration. We applied the method to a thin HZO film grown by ALD on a silicon substrate and retrieved its optical properties without any model assumption with high precision in the energy range of 3.0–6.7 eV. A high precision (≤0.5 Å) on the determination of the film thickness was also shown.

Calculation of the errors enabled to discriminate physical features from artifacts due to systematic or random errors giving additional information on the sensitivity of the measurement, on the whole spectral range. Information on the sensitivity of the measurement in various spectral regions cannot be easily obtained with a standard approach, such as the minimization of the MSE by optimization of the parameters of a Cauchy or Tauc–Lorentz model. With these models, it is harder to determine if a spectral feature has a physical origin and should be considered in the model. The proposed method in this study presents a clear advantage in this regard. Exploiting non-physical exponential dispersions of the thickness, refractive index, and extinction coefficient in the low energy range could improve the accuracy of the measurement. This is especially true in the low energy range where sensitivity to the error is the highest.

The need for a transparency range for thickness determination can be restrictive; it prevents, for example, from studying the first stages of the growth of a metallic compound. However, the constraint in the first step of the method could be overcome by other methods to disambiguate thickness from optical properties. One example is the study of the presence of artifacts in the dielectric constant of the substrate.[12,13] The method proposed in this paper is particularly suited for the study of very thin films of oxides, semiconductors, or 2D materials, either *ex situ* or *in situ* and in real-time, particularly during the first stages of growth. Disambiguating the determination of thickness from the dielectric properties can genuinely improve the information that can be retrieved from spectroscopic ellipsometry measurements.

VI. EXPERIMENTAL DETAILS

Prior to thin film deposition, the silicon substrate is cleaned following a standard RCA procedure to remove organic and ionic contaminations and to obtain a defined oxygen-terminated SiO_x surface with the following steps: SC1: 10 min, 70–80 °C, (5:1:1) $H_2O + NH_4OH$ (29% weight) + H_2O_2 (30% in solution), HF dip: 15 s HF 1%, SC2: 10 min, 70–80 °C, (6:1:1) $H_2O + HCL$ (37% weight) + H_2O_2 (30% in sol.). The samples are rinsed in H_2O and N_2 and blow-dried after each step. This standard RCA cleaning process results in a 1.0 nm (±0.1 nm) chemical oxide SiO_x layer. Before the deposition, the Si/SiO_x stack is measured by ellipsometry to determine ρ_{sub} and define the pseudo-dielectric function that can be used as the substrate dielectric constant $\tilde{n}_{sub}$. The thin film of HZO is deposited on top of the cleaned Si substrate by atomic layer deposition at 250 °C using tetrakis(ethylmethylamino)zirconium (TEMA-Hf) and tetrakis(ethylmethylamino)zirconium (TEMA-Zr) as precursors and de-ionized H_2O as oxidant. The depositions are performed using an "Oxford FlexAl" ALD system. The spectroscopic ellipsometry measurements are made with a Woollam M2000 at an incidence angle of 60°, for a wavelength range of 192–1690 nm corresponding to an energy range of 0.73–6.46 eV. The bulk value of $\tilde{n}_{HZO}$ is determined from a Tauc–Lorentz model on a 20 nm thin film deposited with the same conditions.

SUPPLEMENTARY MATERIAL

See the supplementary material for a detailed mathematical implementation of the Newton–Raphson iterative process. We also

provide in the supplementary material a comparison of our algorithm with a classic model relying on the MSE minimization approach for the theoretical case of a TiO_2 thin film on a Si substrate.

ACKNOWLEDGMENTS

The experimental work was performed in the framework of GraFOx II, a Leibniz-ScienceCampus partially funded by the Leibniz Association.

AUTHOR DECLARATIONS

Conflict of Interest

The authors have no conflicts to disclose.

Author Contributions

Florian Maudet: Conceptualization (lead); Data curation (lead); Formal analysis (lead); Investigation (lead); Methodology (lead); Project administration (lead); Software (lead); Supervision (lead); Validation (lead); Writing – original draft (lead); Writing – review & editing (supporting). **Charlotte Van Dijck:** Investigation (supporting); Writing – review & editing (supporting). **Muhammad Hamid Raza:** Investigation (supporting); Writing – review & editing (supporting). **Catherine Dubourdieu:** Conceptualization (supporting); Funding acquisition (lead); Writing – review & editing (lead).

DATA AVAILABILITY

An archive file with necessary materials of the findings of this study is openly available in Zenodo at https://doi.org/10.5281/zenodo.7722620. The archive contains a Python code of the algorithm of the proposed method, and two Jupyter notebooks used to generate the data in the paper alongside with the experimental and reference data used for analysis.

REFERENCES

[1]H. Fujiwara, *Spectroscopic Ellipsometry* (John Wiley & Sons, Ltd, Chichester, 2007).
[2]H. G. Tompkins and E. A. Irene, *Handbook of Ellipsometry* (Springer, Berlin, 2005).
[3]J. N. Hilfiker, *In Situ Spectroscopic Ellipsometry (SE) for Characterization of Thin Film Growth* (Woodhead Publishing, 2011).
[4]M. Gilliot, Thin Solid Films **520**, 5568 (2012).
[5]H. Kröncke, F. Maudet, S. Banerjee, J. Albert, S. Wiesner, V. Deshpande, and C. Dubourdieu, J. Vac. Sci. Technol. A **39**, 052408 (2021).
[6]H. Kumagai and K. Toyoda, Appl. Surf. Sci. **82–83**, 481 (1994).
[7]M. Junige, M. Geidel, M. Knaut, M. Albert, and J. W. Bartha, in *2011 Semiconductor Conference Dresden* (IEEE, 2011), pp. 1–4.
[8]H. Wang, X. Jiang, and B. G. Willis, J. Vac. Sci. Technol. A **30**, 01A133 (2012).
[9]A. Mahmoodinezhad, C. Janowitz, F. Naumann, P. Plate, H. Gargouri, K. Henkel, D. Schmeißer, and J. I. Flege, J. Vac. Sci. Technol. A **38**, 022404 (2020).
[10]K. B. Rodenhausen and M. Schubert, Thin Solid Films **519**, 2772 (2011).
[11]I. K. Kim and D. E. Aspnes, J. Appl. Phys. **101**, 033109 (2007).
[12]H. Arwin and D. E. Aspnes, Thin Solid Films **113**, 101 (1984).
[13]K. Flock, Thin Solid Films **455–456**, 349 (2004).
[14]F. L. McCrackin, *NBS Technical Note* (National Bureau of Standards, 1969).
[15]M. Gilliot, Thin Solid Films **542**, 300 (2013).
[16]M. Gilliot, A. Hadjadj, and M. Stchakovsky, J. Vac. Sci. Technol. B **37**, 062925 (2019).
[17]S. Y. Jung and Q.-H. Park, Nanophotonics **8**, 263–270 (2019).
[18]J.-P. Dedieu, *Encyclopedia of Applied and Computational Mathematics* (Springer, Berlin, 2015).
[19]H. H. Ku, J. Res. Natl. Bur. Stand. Sect. C Eng. Instrum. **70C**, 263 (1966).
[20]C. M. Herzinger, B. Johs, W. A. McGahan, J. A. Woollam, and W. Paulson, J. Appl. Phys. **83**, 3323 (1998).
[21]D. E. Aspnes, in *Optical Properties of Solids—New Developments*, edited by B. O. Seraphin (Optics & L, 1976), pp. 801–846.
[22]G. A. Niklasson, C. G. Granqvist, and O. Hunderi, Appl. Opt. **20**, 26 (1981).
[23]R. L. Puurunen, Chem. Vap. Depos. **9**, 249 (2003).
[24]A. Barnasas, C. S. Garoufalis, D. I. Anyfantis, N. Bouropoulos, P. Poulopoulos, D. B. Hayrapetyan, and S. Baskoutas, Atoms **9**, 70 (2021).